AD-F300067

(12)

AD A120045

AD

TECHNICAL REPORT ARBRL-TR-02415

SHOCK IGNITION SENSITIVITY OF MULTIPLY-SHOCKED TNT

V. M. Boyle
D. L. Pilarski

DTIC
ELECTE
OCT 6 1982
S D
B

July 1982

US ARMY ARMAMENT RESEARCH AND DEVELOPMENT COMMAND
BALLISTIC RESEARCH LABORATORY
ABERDEEN PROVING GROUND, MARYLAND

Approved for public release; distribution unlimited.

DTIC FILE COPY

82 09 16 038

Destroy this report when it is no longer needed.
Do not return it to the originator.

Secondary distribution of this report is prohibited.

Additional copies of this report may be obtained from the National Technical Information Service, U. S. Department of Commerce, Springfield, Virginia 22161.

The findings in this report are not to be construed as an official Department of the Army position, unless so designated by other authorized documents.

The use of trade names or manufacturers' names in this report does not constitute indorsement of any commercial product.

UNCLASSIFIED

SECURITY CLASSIFICATION OF THIS PAGE (When Data Entered)

REPORT DOCUMENTATION PAGE		READ INSTRUCTIONS BEFORE COMPLETING FORM
1. REPORT NUMBER Technical Report ARBRL-TR-02415	2. GOVT ACCESSION NO. AD-A120045	3. RECIPIENT'S CATALOG NUMBER
4. TITLE (and Subtitle) SHOCK IGNITION SENSITIVITY OF MULTIPLY-SHOCKED TNT		5. TYPE OF REPORT & PERIOD COVERED Final
		6. PERFORMING ORG. REPORT NUMBER
7. AUTHOR(s) V. M. Boyle D. L. Pilarski		8. CONTRACT OR GRANT NUMBER(s)
9. PERFORMING ORGANIZATION NAME AND ADDRESS US Army Ballistic Research Laboratory ATTN: DRDAR-BLT Aberdeen Proving Ground, MD 21005		10. PROGRAM ELEMENT, PROJECT, TASK AREA & WORK UNIT NUMBERS 1L161102AH43
11. CONTROLLING OFFICE NAME AND ADDRESS US Army Armament Research and Development Command US Army Ballistic Research Laboratory (DRDAR-BL) Aberdeen Proving Ground, MD 21005		12. REPORT DATE July 1982
		13. NUMBER OF PAGES 35
14. MONITORING AGENCY NAME & ADDRESS(if different from Controlling Office)		15. SECURITY CLASS. (of this report) UNCLASSIFIED
		15a. DECLASSIFICATION/DOWNGRADING SCHEDULE

16. DISTRIBUTION STATEMENT (of this Report)

Approved for public release, distribution unlimited.

17. DISTRIBUTION STATEMENT (of the abstract entered in Block 20, if different from Report)

18. SUPPLEMENTARY NOTES

19. KEY WORDS (Continue on reverse side if necessary and identify by block number)

shock ignition
multiple shock waves
TNT sensitivity
ignition

20. ABSTRACT (Continue on reverse side if necessary and identify by block number) (dtc)

The shock ignition sensitivity of pressed TNT was decreased by shocking it with a leading low pressure wave (.2 - 1.0 GPa) which was followed within several microseconds by one or two shock waves which gave a maximum pressure of 2.7 GPa. The velocity of the reaction products from the downstream free surface of the impacted TNT was used as a measure of relative reaction. A system is described for producing a series of shocks of increasing amplitude within a target by impacting it with a layered projectile. Several firings were also made using

DD FORM 1 JAN 73 1473 EDITION OF 1 NOV 65 IS OBSOLETE

UNCLASSIFIED

SECURITY CLASSIFICATION OF THIS PAGE (When Data Entered)

20. ABSTRACT (continued)

cast TNT. The results of these firings indicate that the shock ignition sensitivity of cast TNT is also decreased by multiple shocking.

TABLE OF CONTENTS

		Page
	LIST OF ILLUSTRATIONS	5
	LIST OF TABLES	7
	NOTATION	9
I.	INTRODUCTION	11
II.	EXPERIMENT	11
III.	ANALYSIS	12
IV.	RESULTS	17
V.	MANGANIN FOIL PRESSURE GAGE MEASUREMENTS	22
VI.	DISCUSSION	26
VII.	CONCLUSIONS	28
	LIST OF REFERENCES	31
	DISTRIBUTION LIST	33

DTIC COPY INSPECTED

Accession For
NTIS GRA&I ☑
DTIC TAB ☐
Unannounced ☐
Justification
By
Distribution/
Availability Codes
Dist | Avail and/or Special
A

LIST OF ILLUSTRATIONS

Figure		Page
1.	Experimental arrangement	11
2.	Impedance match solution for the first shock wave in TNT and polyethylene	13
3.	Impedance match solution for the first shock wave in Teflon	14
4.	Impedance match solution for the second shock wave in TNT	15
5.	Simplified representation of main shock trajectories in TNT and projectile face plates during the impact process	16
6.	Impedance match solution for the third shock wave in polyethylene	16
7.	Impedance match solution for the third shock wave in TNT	17
8.	Typical pressure pulse shapes in TNT (calculated)	17
9.	Explosive reaction caused by shock wave overtake	18
10.	Free surface velocity of singly-shocked TNT	18
11.	Effect of peak pressure on reaction in double pulse experiments	19
12.	Comparison of the effect of double and triple shock pulses on the explosive	19
13.	Effect of initial pulse duration on reaction	20
14.	The measured and calculated free surface velocities of shocked pressed TNT	21
15.	The measured and calculated free surface velocities of shocked cast TNT	21
16.	Experimental arrangement for measuring the impact pressure using a manganin foil pressure gage	23

LIST OF ILLUSTRATIONS (continued)

Figure Page

17. A comparison of the calculated and measured shock pressure in pressed TNT. 24

18. A comparison of the calculated and measured shock pressure in cast TNT 25

LIST OF TABLES

Number		Page
I	Summary of Pressure Pulse and Free Surface Velocity Data (pressed TNT)	29
II	Summary of Pressure Pulse and Free Surface Velocity Data (cast TNT)	30
III	Comparison of Calculated and Measured Pressures	30

NOTATION

The subscript 1 refers to TNT. Thus,

ρ_1 = initial density of TNT charge

u_1 = particle velocity of first shock wave in TNT

U_1 = velocity of 1st shock wave in TNT

P_1 = pressure of first shock wave in TNT

The subscripts 2, 3, 4 refer to the projectile face plates in order of proximity to the TNT charge. Thus, for the illustration in Figure 2,

u_2 = particle velocity in polyethylene (poly)

u_3 = particle velocity in Teflon

u_4 = particle velocity in aluminum

P_2 = pressure in polyethylene

The superscript ' refers to the singly-shocked material. Thus,

ρ_1' = density of singly-shocked TNT

ρ_2' = density of singly-shocked polyethylene

u_1' = particle velocity with respect to singly-shocked TNT; i.e., the change in particle velocity in the second shock in TNT

u_2' = particle velocity with respect to singly-shocked polyethylene

P_1' = increase in pressure due to second shock wave in TNT

The superscript " refers to the doubly-shocked material. Thus,

u_1'' = particle velocity with respect to doubly-shocked TNT

u_2'' = particle velocity with respect to doubly-shocked polyethylene

P_1'' = increase in pressure due to third shock wave in TNT

To simplify calculations, the density of the shocked material is kept constant at the value it obtained by the primary shock compression. Thus,

$\rho_1'' = \rho_1'$

$\rho_2'' = \rho_2'$

$\rho_3'' = \rho_3'$

I. INTRODUCTION

From shock-initiation-to-detonation experiments, we know that a leading, relatively low pressure shock wave can desensitize an explosive to a following, higher pressure shock wave. In the case reported in reference (1), a 3.9 GPa shock in plastic-bonded HMX desensitized it to a 10 GPa shock which followed one μsec later. This suggests that multiple shocking may be effective in desensitizing explosives to shock ignition also, since shock ignition is highly dependent on the physical structure of the explosive charge. Thus, charges which contain voids are more sensitive than those which do not. Also, larger voids are more sensitizing than smaller ones (2). Under shock compression, these discontinuities within the explosive become the sites of hot spots which can cause ignition under appropriate conditions determined by pressure, temperature, and time.

II. EXPERIMENT

In most of the experiments reported here, the explosive used was pressed TNT, similar to that of reference (2); our density was 1.53 gm/cm^3 whereas that of reference (2) was 1.55 gm/cm^3. The powder used for pressing consisted of grains which passed through a number 50 U.S. standard sieve screen and were retained on a number 70 screen. The experimental arrangement, shown in Figure 1, consists of a 10 cm diameter light gas gun which accelerates a flat-faced projectile toward the TNT charge in the target chamber. The TNT charge is 76.2 mm diameter x 12.7 mm thick. The gun barrel and target chamber are evacuated to a pressure of 50 microns Hg beforehand in order to facilitate projectile acceleration and to minimize the overpressure in the target chamber after firing. The

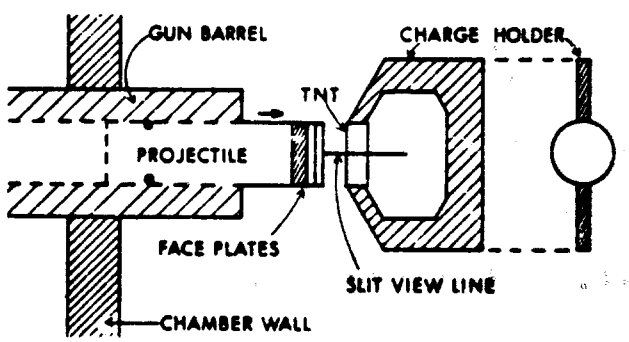

Figure 1 - Experimental Arrangement.

charge holder consists of Plexiglas 12.7 mm thick which is machined so that it supports the charge with minimal confinement; the charge is held in place with epoxy cement. Indicated in Figure 1 is the "slit view

line." This is the area of the event viewed by a continuous recording streak camera, Beckman and Whitley Model 339. Not shown in Figure 1 is a backlighting source, Cordin Model 607, used to form a silhouette of the projectile and charge so that the non-luminous impact event can be recorded by the streak camera. The projectile velocity and downstream free surface velocity of the TNT charge are derived by differentiating the distance-time streak camera data. The face of the aluminum projectile can be left bare to produce a single shock in the explosive or several plates of different materials can be attached to the projectile face to produce multiple shocks in the explosive due to shock reflections at plate interfaces. In these experiments, the downstream free surface velocity of the impacted TNT can be used as an indication of explosive reaction because the gaseous reaction products will have a higher velocity than the unreacted solid explosive.

III. ANALYSIS

The standard impedance matching technique (3) is used to calculate the impact pressure in TNT when a single shock wave is produced. For multiple shock waves, the calculations are more complicated and so they will be described here in some detail. The Hugoniots of materials used are shown in the form $U = a + bu$ where U is shock velocity (mm/μsec), u is particle velocity (mm/μsec) and a and b are empirical constants; density, ρ, is in grams/cm^3.

polyethylene (poly), $\rho = .92$, $U = 2.722 + 1.583\ u$ (4)

Teflon, $\rho = 2.24$, $U = 1.83 + 2.07\ u$ (5)

aluminum, $\rho = 2.785$, $U = 5.355 + 1.345\ u$ (6)

brass, $\rho = 8.45$, $U = 3.781 + 1.431\ u$ (5)

CMW 1000, $\rho = 16.84$, $U = 3.94 + 1.32\ u$ (5)

polyurethane (PU), $\rho = 1.265$, $U = 2.486 + 1.577\ u$ (7)

rigid porous polyurethane, $\rho = .577$, $U = .0087 + 1.8179\ u$

cast TNT, $\rho = 1.614$, $U = 2.39 + 2.05\ u$ (5)

porous TNT, $\rho = 1.53$, $U = .89 + 5.27\ u$

CMW 1000 is a sintered alloy consisting of 90 percent W, 4 percent Cu, 6 percent Ni (8). The porous Hugoniots for polyurethane and TNT were generated using the procedure described in reference (9) with the following

values of Grüneisen Gamma, Γ_o:

For TNT, $\Gamma_o = .737$ (9)

For polyurethane, $\Gamma_o = 1.55$ (10)

The porous Hugoniots shown are for the pressure range 0 - 1 GPa. The porous TNT Hugoniot is used to calculate the pressure and particle velocity produced by the first shock wave. The higher-density, cast TNT Hugoniot is used for the second and third shock waves which interact with shock-compressed TNT.

In a coordinate system where the projectile is at rest, the impact process can be described as shown in Figure 2 where the Hugoniot curves of several materials are drawn in the pressure-particle velocity plane. The free surface velocity of TNT, u_{FS}, is equal to the projectile velocity. At the impact interface of TNT and poly, the pressure and

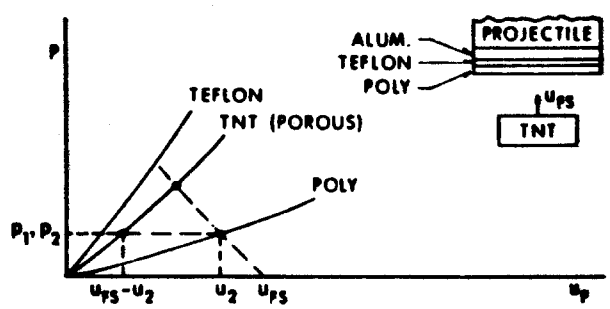

Figure 2 - Impedance match solution for the first shock wave in TNT and polyethylene.

particle velocity are equal. Therefore we can write

$$P_2 = P_1 \quad (1)$$

$$\rho_2 U_2 u_2 = \text{func. } (u_{FS} - u_2) \quad (2)$$

$$\rho_2(a_2 + b_2u_2)u_2 = \rho_1\left[a_1 + b_1(u_{FS} - u_2)\right](u_{FS} - u_2) \quad (3)$$

This reduces to a quadratic equation which can be solved for u_2. Knowing u_2, we can calculate P_1, the pressure of the first shock wave in TNT.

Also, $2u_2$ represents the free surface velocity of poly with respect to the Teflon plate. So, referring to Figure 3, we can write

$$\rho_3(a_3 + b_3u_3)u_3 = \rho_2\left[a_2 + b_2(2u_2 - u_3)\right](2u_2 - u_3) \quad (4)$$

This reduces to a quadratic equation which can be solved for u_3, the particle velocity in Teflon. This procedure can be repeated to find the particle velocity and pressure at each interface of the layered plate.

In order to calculate the pressures produced in TNT by these reflected interface pressures we can, referring to Figure 3, proceed as follows. At the poly-Teflon interface, a shock reflection takes place, the pres-

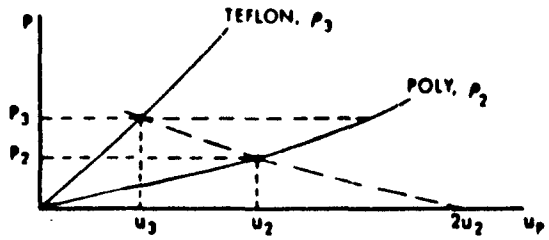

Figure 3 - Impedance match solution for the first shock wave in Teflon.

sure jumps ΔP, the particle velocity decreases by $u_2 - u_3$ and the reflected shock travels back into the shock-compressed poly of density ρ_2'

$$\Delta P = P_3 - P_2 = P_2' \tag{5}$$

P_2' can also be calculated in the following manner:

For the reflected shock wave traveling back into the previously shocked polyethylene the assumption is made that the pressure can be represented by

$$P_2' = \rho_2' \left[a_2 + b_2 (u_2 - u_3)\right] (u_2 - u_3) \tag{6}$$

where the Hugoniot of the shock-compressed polyethylene was approximated by

$$U_2' = a_2 + b_2 (u_2 - u_3) \tag{7}$$

and the density of the shock-compressed polyethylene was calculated as

$$\rho_2' = \rho_2 \left(\frac{U_2}{U_2 - u_2}\right) \tag{8}$$

using values of U_2, u_2 and u_3 calculated from the preceding section. The

Hugoniot constants a_2 and b_2 are those of unshocked polyethylene. Equation (5) represents an upper bound on the calculated pressure jump and equation (6) a lower bound. We have chosen to use equation (6) in our analysis.

Knowing $u_2' = u_2 - u_3$ we can perform an impedance matching calculation in order to calculate u_1', the particle velocity in singly-shocked TNT produced by the reflected shock wave originating at the poly-Teflon interface. Figure 4 represents the impedance match calculation for the first shock reflection from the poly-Teflon interface back into singly shocked TNT. The particle velocities are relative to the polyethylene-TNT interface velocity caused by the initial shock wave. Referring to

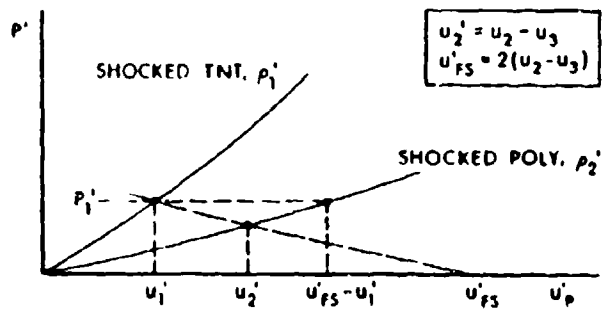

Figure 4 - Impedance match solution for the second shock wave in TNT.

Figure 4, we can write the following equation.

$$P_1' = \rho_1' \, (a_1 + b_1 u_1') \, u_1' =$$

$$\rho_2' \left[a_2 + b_2 (2u_2 - 2u_3 - u_1') \right] (2u_2 - 2u_3 - u_1') \qquad (9)$$

This reduces to a quadratic equation which can be solved for u_1'.

$$\text{For TNT } u_{MAX} = u_1 + u_1'$$

$$P_{MAX} = P_1 + P_1'$$

When three plates are used, the impedance matching solution must take into account the first shock reverberation in poly which gets reflected at the poly-TNT interface as shown at A in Figure 5. B represents a second shock reverberation in poly of small magnitude; for simplicity we have ignored it in our calculations. The effect of the reflection at A is to shift the impedance matching line of symmetry

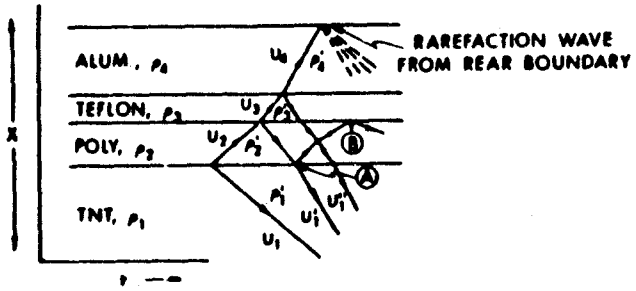

Figure 5 - Simplified representation of main shock trajectories in TNT and projectile face plates during the impact process.

from (u_3-u_4) to $(u_3-u_4 + \Delta u)$ where $\Delta u = (u_2-u_3-u_1')$. The net result is a higher transmitted pressure P_1'' in TNT. Referring to Figure 6 which

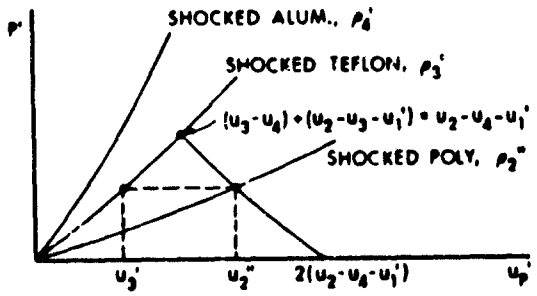

Figure 6 - Impedance match solution for the third shock wave in polyethylene.

shows the impedance matching solution for the third shock wave in poly we can write the following quadratic equation

$$\rho_2''(a_2+b_2u_2'')\,u_2'' =$$

$$\rho_3'\left[a_3+b_3\,(2u_2-2u_4-2u_1'-u_2'')\right]$$

$$(2u_2-2u_4-2u_1-u_2'') \qquad (10)$$

which can be solved for u_2'', the particle velocity in doubly shocked poly caused by the shock wave reflected at the Teflon-aluminum interface.

Using u_2'', a final application of the impedance matching technique

at the interface of doubly-shocked poly and TNT can be made as shown in Figure 7.

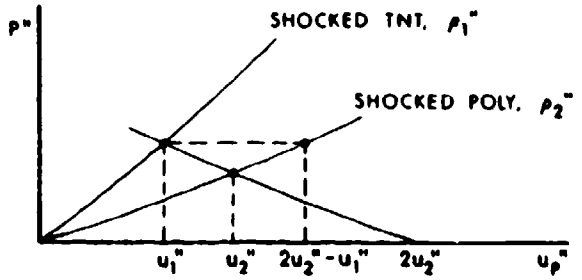

Figure 7 - Impedance match solution for the third shock wave in TNT.

Equating pressures, we can write the quadratic equation

$$\rho_1''\left(a_1+b_1u_1''\right)u_1'' = \rho_2''\left[a_2+b_2\left(2u_2''-u_1''\right)\right]\left(2u_2''-u_1''\right) \tag{11}$$

which can be solved for u_1, the particle velocity in doubly-shocked TNT due to U_1'', the third shock wave in TNT. For TNT,

$$u_{MAX.} = u_1+u_1'+u_1''$$

$$P_{MAX.} = P_1+P_1'+P_1''$$

IV. RESULTS

Figure 8 illustrates several typical pressure profiles in TNT calcu-

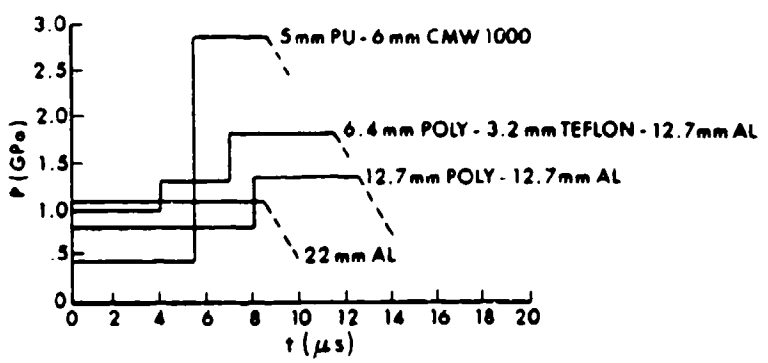

Figure 8 - Typical pressure pulse shapes in TNT (calculated).

lated by the procedures outlined in the preceding section. The time duration of pressure at each level is simply the reverberation time of a shock wave in the face plate associated with a given pressure level in TNT. The pulse shapes shown in Figure 8 represent the maximum duration each pressure pulse will have at the TNT-poly interface. The second and third shock waves propagating in shock-compressed TNT will tend to catch up with the relatively slower primary shock wave propagating in porous TNT so that the time difference between the first and second shock waves will become less as the waves propagate into the TNT sample. In some of our early firings where 3.2 mm thick poly was used as the first plate (2μsec reverberation time) the second shock wave overtook the first wave causing a drastic increase in explosive reaction. This situation is illustrated in Figure 9. The overtake was prevented by increasing the thickness of the first plate to 6.4 mm, giving a 4 μsec

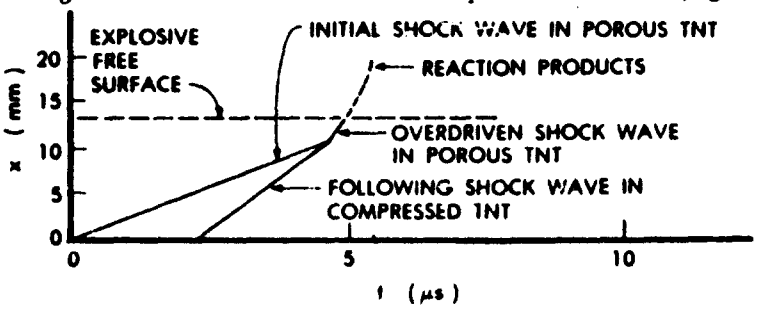

Figure 9 - Explosive reaction caused by shock wave overtake.

interval between the first and the second shock waves in TNT.

Figure 10 shows the free surface velocity of singly-shocked TNT.

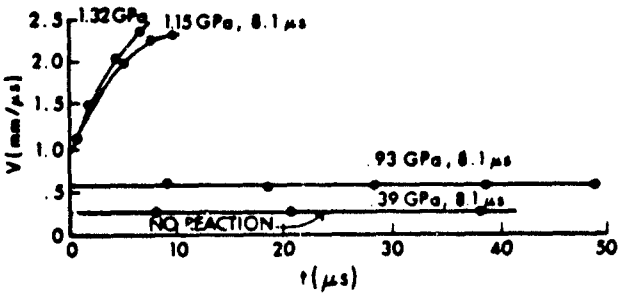

Figure 10 - Free surface velocity of singly-shocked TNT.

Each curve is labeled to show the pressure and pulse width of the shock wave in TNT. For the 0.39 GPa curve, the free surface velocity is constant and unreacted explosive was recovered from the target chamber. The free surface velocity for the 0.93 GPa impact pressure is also quite constant but in this case the target chamber was covered with soot indi-

cating that a comparatively mild reaction must have occurred. Both the 1.15 and 1.32 GPa curves show an accelerating free surface indicating that significant explosive reaction is occurring. The maximum velocity recorded was 2.7 mm/μsec, just before the free surface left the streak camera field of view. For comparison, the reaction products velocity at 50 μ Hg from a detonating TNT charge is 9 mm/μsec.

Figure 11 shows the measured free surface velocity of doubly-shocked

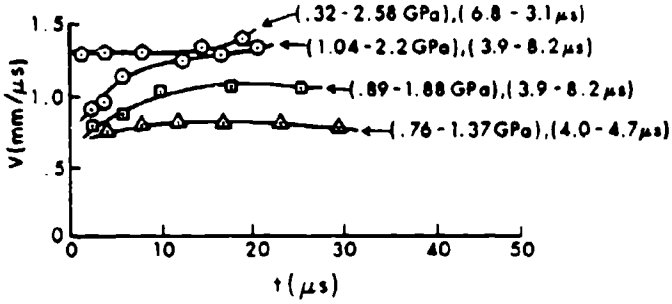

Figure 11 - Effect of peak pressure on reaction in double pulse experiments.

TNT. In all cases, there was explosive reaction as evidenced by soot formation in the target chamber. However, the free surface velocities are considerably below the level reached when a single shock of comparable pressure is used. The free surface velocity, in general, increases as the maximum pressure increases. Referring to the curve showing an 0.32 GPa initial pressure, it can be seen that the free surface velocity is slowly increasing. In this case, the pressure of the first shock is too low to cause reaction as shown by the case of a single shock wave in TNT at 0.39 GPa. This would imply that the reaction is due to the interaction of the second shock wave with TNT.

Figure 12 compares the effects of double and triple shock pulses on the explosive. These curves compare the free surface velocities produced by a double pulse to that by a triple pulse at the pressure levels and times indicated. Although we were not able to match initial and final pulses exactly, the data show no obvious effect due to the intermediate shock.

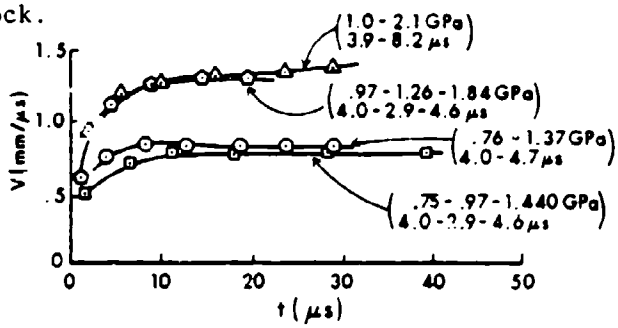

Figure 12 - Comparison of the effect of double and triple shock pulses on the explosive.

Figure 13 compares the effect of the duration of the initial shock

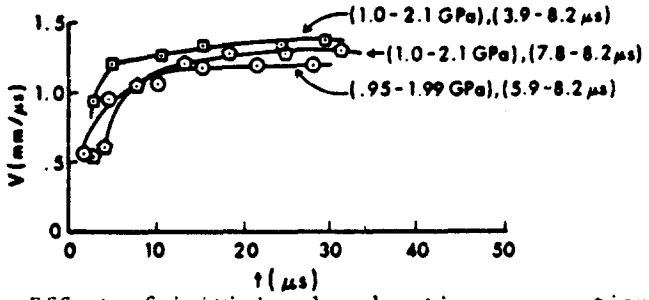

Figure 13 - Effect of initial pulse duration on reaction.

pulse on the velocity of the reaction products. There appears to be no significant difference except that a longer initial pulse delays the increase in free surface velocity as would be expected if the first shock wave were substantially unreactive.

Figure 14 compares the measured free surface velocity with that calculated for unreacted pressed TNT of 1.53g/cm^3 density. The numbers correspond to shot numbers shown in Table I. The unreacted free surface velocities were calculated as

$$V = 2u_1, \text{ for a single shock,}$$

$$V = 2(u_1 + u_1') \text{ for a double shock,}$$

$$V = 2(u_1 + u_1' + u_1'') \text{ for a triple shock.}$$

For singly-shocked pressed TNT, there is a big difference between the calculated and measured values of the free surface at 1.15 GPa and very little difference at 0.93 GPa. We interpret this to mean that prompt ignition of the TNT occurs at a shock pressure between these levels.

For multiply shocked TNT, it can be seen that there is little difference between measured and calculated free surface velocities at the 1.5 GPa level. Also, the difference beween measured and calculated free surface velocities increases gradually with maximum shock pressure. This indicates that pre-shocking pressed TNT desensitizes it to shock ignition by successive shock waves of higher pressure.

A small number of firings were made using cast TNT explosive to see if multiple shock desensitizing was effective for cast explosives as well. Figure 15 compares the measured free surface velocity with that calculated for unreacted cast TNT of 1.61 g/cm^3 density. The numbers correspond to shot numbers shown in Table II. From the difference in free surface velocity, it can be seen that there is very little reaction at 0.97 GPa and extensive reaction at 2.53 GPa for a single shock wave.

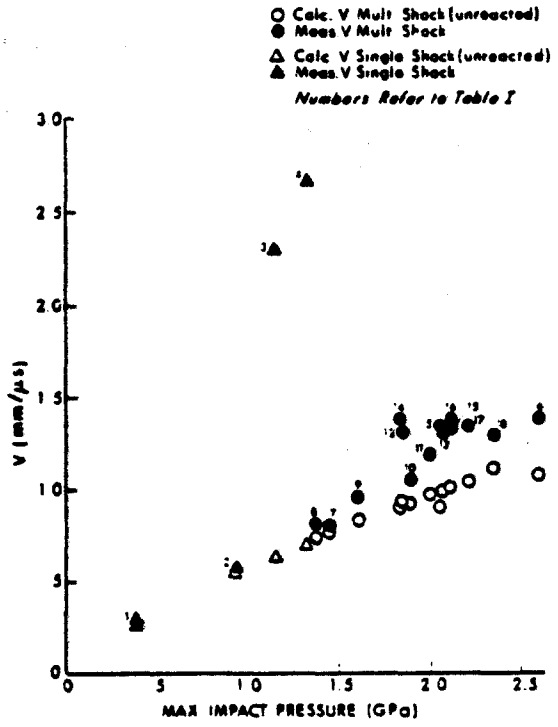

Figure 14 - The measured and calculated free surface velocities of shocked pressed TNT.

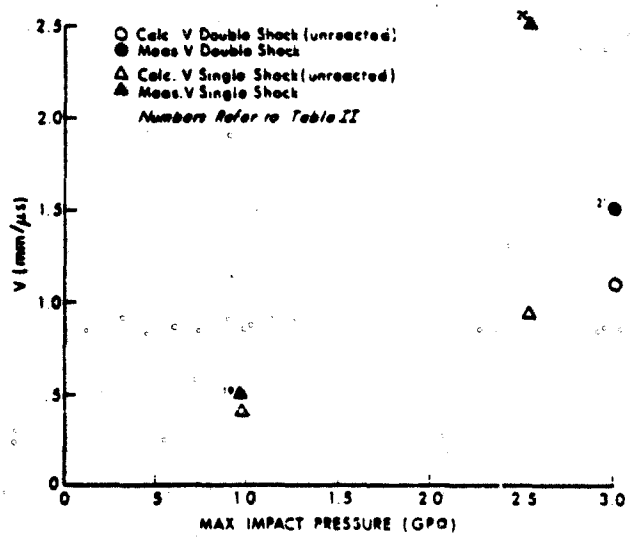

Figure 15 - The measured and calculated free surface velocities of shocked cast TNT.

However, a double shock wave having a maximum pressure of 3.0 GPa produces only moderate reaction. This indicates that pre-shocking cast TNT desensitizes it to shock ignition by successive shock waves of higher pressure.

V. MANGANIN FOIL PRESSURE GAGE RESULTS

Toward the end of this program we decided to make shock pressure measurements both as a check on the impedance matching calculations and for the observation of developing reaction at the front surface of our explosive sample. The experimental setup is shown in Fig. 16. A fifty ohm manganin foil pressure gage was sandwiched between two 0.20 mm thick Mylar sheets along with a thin layer of RTV silicone rubber compound. This sandwich was then fastened to the front surface of the explosive charge using RTV silicone rubber compound. The gage leads left the charge along the 45° beveled surface; it was felt that this configuration would provide longer gage life under shock loading. The manganin foil pressure gage formed one leg of a Wheatstone bridge circuit as shown in Fig. 16. The input to the bridge circuit was 180 volts provided by a K-Line Corp. Pulse Power supply. The output from the bridge circuit went to a Nicolet model 204A waveform recorder. The pressure sensitivity of the Micro-Measurements gages used was 0.027 ohm/ohm/GPa. The output signal voltage from the Wheatstone bridge circuit can be related to the shock pressure through the following equation,

$$P = \frac{4}{(0.027)\left(\frac{e}{\Delta v} - 2\right)} \qquad (12)$$

where Δv = signal voltage (volts)
e = input voltage (volts)
P = shock pressure (GPa).

Fig. 17 compares measured and calculated shock pressures for pressed TNT. It can be seen that for the single shock the measured pressure is about 88% of the calculated value. Also the pressure at the impacted face is increasing with time. The gage broke after 5 microseconds. The double shock experiment indicates that the measured pressures are 82% and 76% of the calculated values for the first and second shock wave respectively. There is no indication of reaction until about 0.5 μsec after the high pressure wave enters the shocked explosive.

Fig. 18 shows the response of cast TNT to single and double shock waves. For the single shock waves the measured pressure is about 85% of the value calculated by impedance matching. There is evidence of explosive reaction at the impacted surface as shown by the increase of pressure with time. The reaction rate increases with the impact pressure. The double shock wave experiment showed that the measured pressures

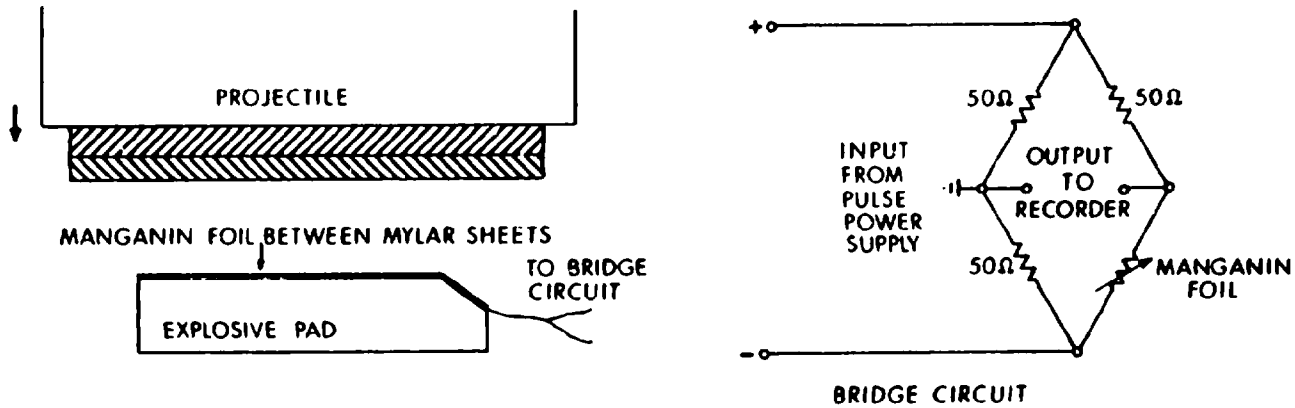

Figure 16 - Experimental arrangement for measuring the impact pressure using a manganin foil pressure gage.

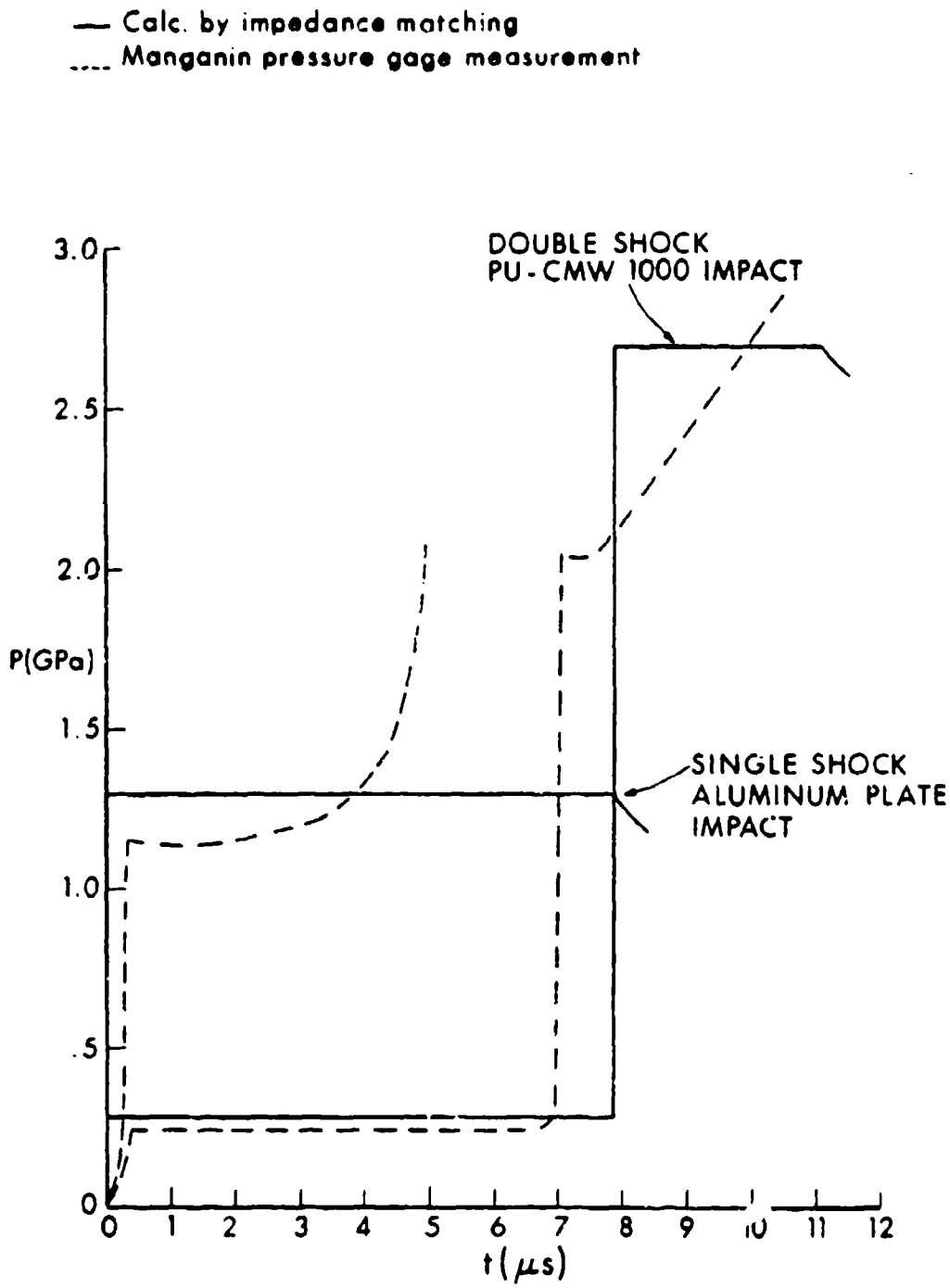

Figure 17 - A comparison of the calculated and measured shock pressure in pressed TNT.

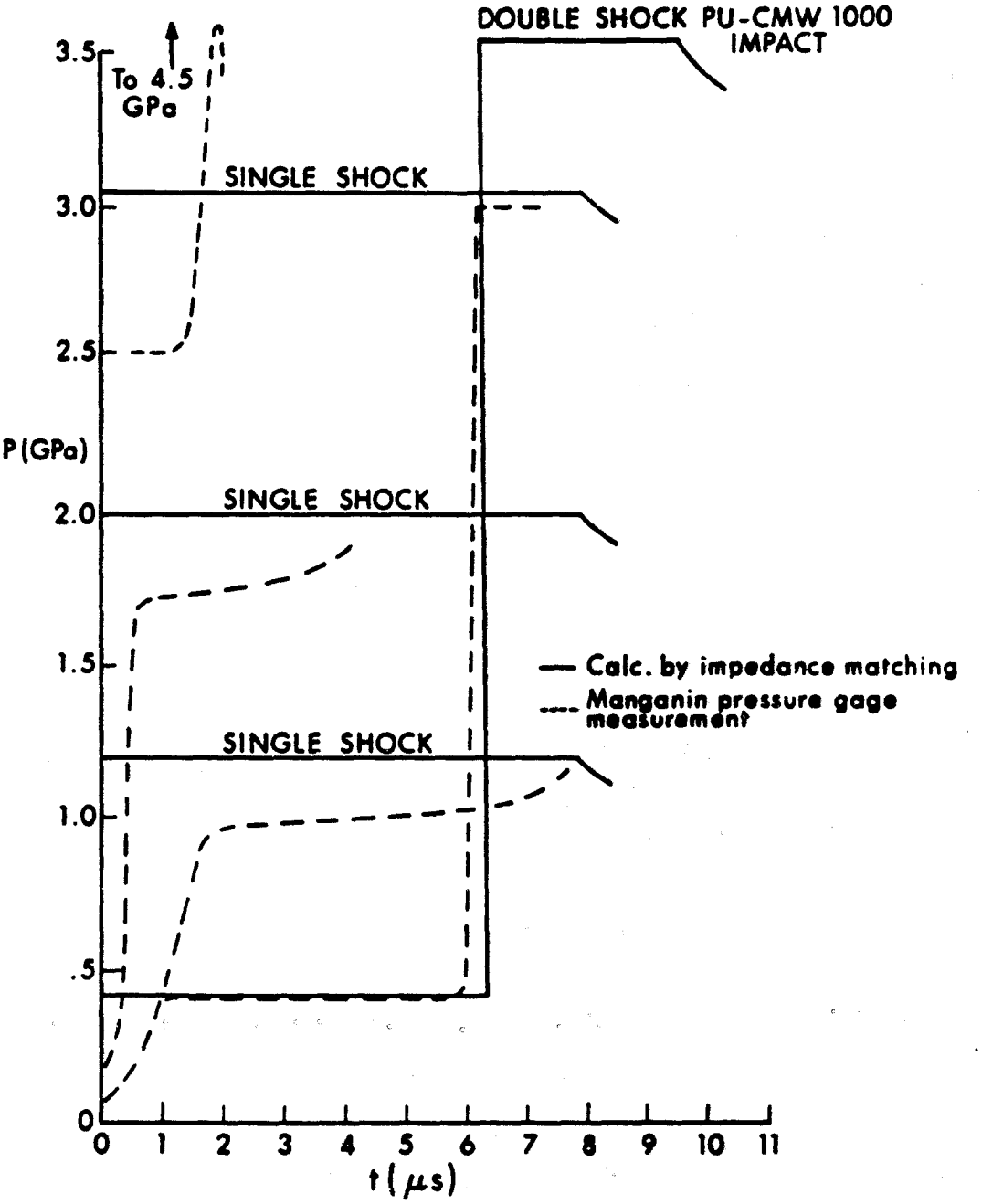

Figure 18 - A comparison of the calculated and measured shock pressure in cast TNT.

are 95% and 85% of the calculated pressures for the first and second shock wave respectively. There is no indication of explosive reaction, The manganin gage broke after seven microseconds. A comparison of measured and calculated shock pressures for the six shots using manganin gages is shown in Table III.

VI. DISCUSSION

Referring to Fig. 14 and Table I, it can be seen that shots 12 and 14 give a higher reaction product velocity than shot 10 which has a comparable maximum pressure. Shots 12 and 14, however, have higher initial pressures which may be causing significant reaction. If this is so, the initial pressure should be limited to values below 0.9 GPa in order to achieve effective desensitization by double shocking. Also, an initial pressure as low as 0.23 GPa was effective in desensitizing pressed TNT to a following shock wave of 2.05 GPa as shown by shot 5.

For cast TNT we do not have as much data but from the manganin gage pressure measurements shown in Fig. 18 and Table II it can be seen that cast TNT is reacting at a shock pressure of 0.97 GPa. The initial pressure should probably be limited to values below 0.9 GPa for effective desensitization. Also a pressure as low as 0.4 GPa proved effective in desensitizing cast TNT to a following shock wave of 3.0 GPa pressure.

As has been noted there is some disagreement between the calculated shock pressures (impedance matching) and the measured shock pressures (manganin foil gage) with the measured pressures being approximately 85% of the calculated pressures. The pressure sensitivity of the gages used in these experiments was 0.027 ohm/ohm/GPa. It can be seen by referring to equation 12 that a lower pressure sensitivity value would yield higher pressure values. Alternatively, the pressures calculated by impedance matching could be lowered if different Hugoniot constants were used for the plates and explosive samples. We have accepted the gage data as being a more direct measure of the shock pressure. Several of the shots, listed in Table I were corrected by gage data obtained on similar shots.

Our experiments comparing the results of double and triple shock waves on explosive reaction, Fig. 12, indicate no obvious difference. In retrospect, this is not surprising since voids in the explosive sample are rapidly collapsed by the first shock and subsequent shocks encounter a void-free explosive. The void size in our pressed TNT samples was estimated from SEM photographs to be around 10 microns. The void closure time under shock loading was estimated to be around 0.01 microsecond which is much less that the time between shock waves in our multiple shock experiments. For the same reason, the duration of the initial shock wave, Fig. 13, had no discernible effect on the

degree of reaction produced. In our multiple shock experiments, there was always some reaction but at a reduced level compared to a single shock of the same magnitude and the level of reaction increased with the maximum impact pressure. As the first shock wave approached 1.0 GPa, the measured reaction products velocity appeared higher than would be expected for the final maximum pressure (shots 12 and 14). This may indicate that the first shock is of sufficient magnitude to cause significant reaction; the manganin gage results support this hypothesis.

In the multiple shock experiments reported here, the effect of the first shock wave was to make the explosive less sensitive to shock ignition. This was probably accomplished by shock compaction of the TNT into the void volume, making a more nearly homogeneous charge, substantially free of potential hot spot ignition sites. There are cases, however (11), where the effect of a leading shock wave is to make an explosive charge more sensitive to ignition. In experiments reported in reference (11), a leading low pressure shock wave in cast TNT made it more sensitive to detonation by a second shock when the time between the first and second shocks was about 10 μsec. This was attributed to the effect of the negative pressure wave, associated with the first shock wave, which altered the explosive charge structure causing it to become more heterogeneous.

In reference (12), evidence is presented that there is a minimum shock energy per unit mass (critical specific energy) required for ignition; this energy is independent of the original explosive density over a wide range of densities. However, the critical specific energy will depend on the pressure pulse duration; in general, a longer pulse duration will require a lower critical specific energy for ignition. Knowing the explosive Hugoniot we can convert the minimum pressure required to ignite TNT to a critical specific energy.

$$E^1 = \frac{Pu_p}{\rho o\, U_s} = \frac{\rho o\, U_s u_p^2}{\rho o\, U_s} = u_p^2$$

where E' = critical specific energy (ergs/gm)

P = pressure (dynes/cm^2), 1 GPa = 10^{10} dynes/cm^2

ρo = original explosive density (gm/cm^3)

U_s = shock velocity in explosive (cm/sec)

u_p = particle velocity in explosive (cm/sec)

In shot 2 (P= .93 GPa, t = 8.1 μsec), the explosive reacted but the free surface velocity remained constant indicating that the reaction was not very energetic. If we assume this shot represents conditions very close to marginal ignition, then the critical specific energy required to ignite TNT is 7.0 x 10^8 ergs/gm when the pressure pulse duration is around 8 μsec.

VII. CONCLUSIONS

A. A leading low pressure shock wave is effective in suppressing shock ignition in both pressed and cast TNT. Shock ignition is not eliminated entirely but the degree of reaction is moderated.

B. Initial shock waves in the .2 GPa - .9 GPa range are effective in suppressing shock ignition.

C. For pressure pulse durations around 8 μsec, the critical specific energy to ignite TNT is 7×10^8 ergs/gm.

TABLE I

Summary of Pressure Pulse and Free Surface Velocity Data (pressed TNT)

No.	P_1 (GPa)	t_1 (μsec)	P_1' (GPa)	t_1' (μsec)	P_1'' (GPa)	t_1'' (μsec)	$P_{MAX.}$ (GPa)	$V_{CALC.}$ (mm/μsec)	$V_{MEAS.}$ (mm/μsec)
1*	.39	8.1	-	-	-	-	.39	.29	.26
2*	.93	8.1	-	-	-	-	.93	.54	.56
3	1.15	8.1	-	-	-	-	1.15	.63	2.30
4*	1.32	8.1	-	-	-	-	1.32	.70	2.66
5	.23	7.9	1.82	3.1	-	-	2.05	.90	1.34
6*	.32	6.9	2.26	3.1	-	-	2.58	1.07	1.38
7	.75	4.0	.22	2.9	.47	4.6	1.44	.77	.79
8	.76	4.0	.61	4.7	-	-	1.37	.73	.81
9	.77	3.9	.83	8.2	-	-	1.60	.82	.95
10	.89	3.9	.99	8.2	-	-	1.88	.92	1.06
11	.95	5.9	1.04	8.2	-	-	1.99	.96	1.19
12	.97	4.0	.29	2.9	.58	4.6	1.84	.93	1.30
13	.99	3.9	1.08	8.2	-	-	2.07	.99	1.30
14	1.00	4.0	.82	4.7	-	-	1.82	.90	1.37
15	1.00	7.8	1.10	8.2	-	-	2.10	1.00	1.32
16	1.00	3.9	1.10	8.2	-	-	2.10	1.00	1.38
17	1.04	3.9	1.16	8.2	-	-	2.20	1.03	1.33
18	1.05	3.8	1.29	3.1	-	-	2.34	1.11	>1.29

*These pressures were obtained by adjusting impedance match calculations on the basis of manganin pressure gage measurements.

TABLE II

Summary of Pressure Pulse and Free Surface Velocity Data (Cast TNT)

No.	P_1 (GPa)	t_1 (μsec)	P_1' (GPa)	t_1' (μsec)	$P_{MAX.}$ (GPa)	$V_{CALC.}$ (mm/μsec)	$V_{MEAS.}$ (mm/μsec)
19	.97	8	-	-	.97	.42	.51
20	1.71	8	-	-	1.71	.69	no record
21	2.53	8	-	-	2.53	.94	2.51
22	.40	6.3	2.60	3.2	3.00	1.10	1.52

The pressures shown are those obtained from maganin foil pressure gage measurements.

TABLE III

Comparison of Calculated and Measured Pressures

Shot No.	Calculated Pressure Impedance Matching (GPa)	Meas. Pressure Manganin Gage (GPa)	$\frac{\text{Meas.}}{\text{Calc.}} \times 100$
3	1.3	1.15	88%
5	.28-2.70	.23-2.05	82%-76%
19	1.2	.97	81%
20	2.0	1.71	86%
21	3.05	2.53	83%
22	.42-3.55	.40-3.00	95%-85%

REFERENCES

1. A. W. Campbell, et al, "Shock Initiation of Solid Explosives," The Physics of Fluids, Vol. 4, No. 4, pp 511-521, April 1961.

2. B. C. Taylor and L. H. Ervin, "Separation of Ignition and Buildup to Detonation in Pressed TNT," Proceedings of Sixth Symposium on Detonation, pp 3-10, August 1976.

3. M. H. Rice, et al, Solid State Physics (Advances in Research and Applications), Vol. 6, Seitz and Turnbull, eds., pp 1-63, Academic Press, New York 1958.

4. Private communication from G. E. Hauver, Ballistics Research Laboratory, Aberdeen Proving Ground, Maryland.

5. Compendium of Shock Wave Date, M. Van Thiel, et al, eds., UCRL 50108, Vol II.

6. Compendium, Vol. I.

7. Compendium, Vol II. A linear fit was made to the 14 lowest data points of this reference.

8. CMW 1000 was furnished by Contacts Metals Welding Inc., Indianapolis, Indiana.

9. J. O. Erkman and D. J. Edwards, "Computed and Experimental Hugoniots for Unreacted Porous Explosives," Proceedings of Sixth Symposium on Detonation, pp 766-776, August 1976.

10. R. M. James, et al, "The Critical Angle for Mach Bridge Formation Between Opposing Shock Waves in Polyurethane Foam," Proceedings of Sixth Symposium on Detonation, pp 489-501, August 1976.

11. S. G. Andreev, et al, "Detonation Initiation in Step Loading," Combustion, Explosion and Shock Waves, pp 102-105, January 1977.

12. P. M. Howe, BRL Memo Report No. 2152 (1970). (AD A519975L)

DISTRIBUTION LIST

No. of Copies	Organization
12	Administrator Defense Technical Info Center ATTN: DTIC-DDA Cameron Station Alexandria, VA 22314
1	Commander US Army Materiel Development and Readiness Command ATTN: DRCDMD-ST 5001 Eisenhower Avenue Alexandria, VA 22333
5	Commander US Army Armament Research and Development Command ATTN: DRDAR-TDC DRDAR-TSS (2 cy) DRDAR-LCE, Dr. R.F.Walker DRDAR-LCE, Dr. N. Slagg Dover, NJ 07801
1	Commander US Army Armament Materiel Readiness Command ATTN: DRSAR-LEP-L, Tech Lib Rock Island, IL 61299
1	Director US Army ARRADCOM Benet Weapons Laboratory ATTN: DRDAR-LCB-TL Watervliet, NY 12189
1	Commander US Army Aviation Research and Development Command ATTN: DRDAV-E 4300 Goodfellow Boulevard St. Louis, MO 63120
1	Director US Army Air Mobility Research and Development Laboratory Ames Research Center Moffett Field, CA 94035
1	Commander US Army Communications Rsch and Development Command ATTN: DRDCO-PPA-SA Fort Monmouth, NJ 07703
1	Commander US Army Electronics Research and Development Command Technical Support Activity ATTN: DELSD-L Fort Monmouth, NJ 07703
1	Commander US Army Missile Command ATTN: DRSMI-R Redstone Arsenal, AL 35898
1	Commander US Army Missile Command ATTN: DRSMI-YDL Redstone Arsenal, AL 35898
1	Commander US Army Missile Command ATTN: DRSME-RK, Dr. R.G. Rhoades Redstone Arsenal, AL 35898
1	Commander US Army Tank Automotive Rsch and Development Command ATTN: DRDTA-UL Warren, MI 48090

DISTRIBUTION LIST

No. of Copies	Organization
1	Director US Army TRADOC Systems Analysis Activity ATTN: ATAA-SL, Tech Lib White Sands Missile Range NM 88002
1	Commander US Army Research Office ATTN: Chemistry Division P.O. Box 12211 Research Triangle Park, NC 27709
1	Commander Office of Naval Research ATTN: Dr. J. Enig, Code 200B 800 N. Quincy Street Arlington, VA 22217
1	Commander Naval Sea Systems Command ATTN: Mr. R. Beauregard, SEA 64E Washington, DC 20362
1	Commander Naval Explosive Ordnance Disposal Facility ATTN: Technical Library Code 604 Indian Head, MD 20640
1	Commander Naval Research Lab ATTN: Code 6100 Washington, DC 20375
1	Commander Naval Surface Weapons Center ATTN: Code G13 Dahlgren, VA 22448
8	Commander Naval Surface Weapons Center ATTN: Mr. L. Roslund, R122 Mr. M. Stosz, R121 Code X211, Lib E. Zimet, R13 R.R. Bernecker, R13 J.W. Forbes, R13 S.J. Jacobs, R10 K. Kim, R13 Silver Spring, MD 20910
4	Commander Naval Weapons Center ATTN: Dr. L. Smith, Code 3205 Dr. A. Amster, Code 385 Dr. R. Reed, Jr., Code 388 Dr. K. J. Graham, Code 3835 China Lake, CA 93555
1	Commander Fleet Marine Force, Atlantic ATTN: G-4 (NSAP) Norfolk, VA 23511
1	AFRPL ATTN: Mr. R. Geisler, Code AFRPL MKPA Edwards AFB, CA 93523
1	Commander Ballistic Missile Defense Advanced Technology Center ATTN: Dr. David C. Sayles P.O. Box 1500 Huntsville, AL 35804
1	University of California Lawrence Livermore Laboratory P. O. Box 808 ATTN: Dr. M. Finger Livermore, CA 94550

DISTRIBUTION LIST

No. of Copies	Organization
1	Director Los Alamos Scientific Lab ATTN: Dr. B. Craig, M Division P.O. Box 1663 Los Alamos, NM 87544
1	Schlumberger Well Services ATTN: Dr. C. Aseltine 5000 Gulf Freeway Houston, TX 77023

Aberdeen Proving Ground

Dir, USAMSAA
ATTN: DRXSY-D
DRXSY-MP, H. Cohen
Cdr, USATECOM
ATTN: DRSTE-TO-F
Dir, USACSL, Bldg 3516, EA
ATTN: DRDAR-CLB-PA